Chapter 2 Synthesis and Characterization Techniques

Two-dimensional transition metal dichalcogenide (TMDs) have gained vibrant worldwide research interest owing to their unique properties, versatility and expansive applications. Through a combination of experimental and theoretical studies, these materials have unveiled exceptional traits, sparking a revolution in nanomaterials and nanodevices. The TMD family includes various compounds such as MoS_2, $MoSe_2$, WS_2, WSe_2, VS_2, SnS_2, TaS_2, and NbS_2. The MoS_2 stands out as the extensively studied TMD nanomaterial. Among the various synthesis routes, this chapter intends to briefly discuss the optimized growth conditions for the adopted chemical vapor deposition (CVD) technique for the fabrication of different morphologies of MoS_2 over different substrates. Furthermore, the characterization techniques like optical microscopy, scanning electron microscopy (SEM), atomic force microscopy (AFM), Raman, photoluminescence (PL) and UV-visible spectrophotometer, used to analyse prepared materials have been discussed in this chapter.

2.1 Synthesis Methods

Different morphologies of MoS_2 can be obtained using various techniques. Modifications in synthesis route can yield high-quality, uniform and large area MoS_2 with controlled thickness. Synthesis of MoS_2 is mainly categorized based on two approaches: top-down and bottom-up, as shown in **Figure 2.1**. In the former approach, the transformation of the 2D layered bulk nanomaterials into a single or few layers is achieved through physical or chemical processes that includes methods like mechanical exfoliation, liquid phase exfoliation and lithium-ion intercalation. In the bottom-up approach, atomic or molecular precursors undergo reactions to form nanomaterials via direct chemical reaction and this involves techniques such as solution chemical process (hydrothermal, solvothermal and colloidal synthesis), physical vapour deposition [sputtering, pulse laser deposition (PLD) and molecular

beam epitaxy (MBE)] and chemical vapor deposition (CVD). The detailed description of each of these methods have already been outlined in **Chapter 1**.

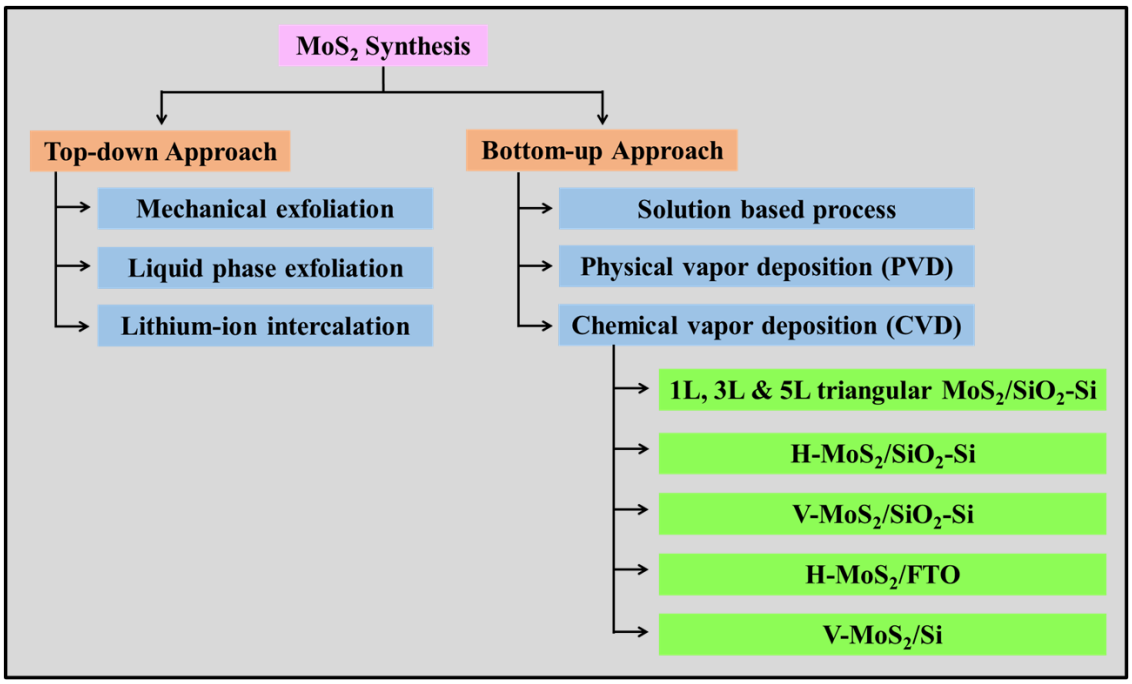

Figure 2.1 *Schematic showing the different synthesis methods of MoS_2.*

In the present work, five different types of MoS_2 films have been prepared via CVD technique with different orientation (horizontally/vertically) grown over different substrates [SiO_2-Si, fluorine-doped tin oxide coated glass (FTO) and Si], as given below:

1) Horizontally grown triangular (1L, 3L and 5L) MoS_2 over SiO_2-Si substrate.
2) Horizontally grown thin film MoS_2 over SiO_2-Si substrate (H-MoS_2/SiO_2-Si).
3) Vertically oriented few layer MoS_2 film grown over SiO_2-Si substrate (V-MoS_2/SiO_2-Si).
4) Horizontally grown thin film MoS_2 over FTO coated glass substrate (H-MoS_2/FTO).
5) Vertically oriented few layer MoS_2 grown over Si substrate (V-MoS_2/Si).

CVD Synthesis of MoS_2 Nanostructures

It is a highly preferred technique for growing large-scale, uniform and high quality TMD nanomaterials with controlled thickness. In this method, the volatile Mo precursors (like MoO_3, $(NH_4)_2MoS_4$ or Mo) decompose and deposit on the desired substrate at high temperature

in the presence of an inert atmosphere, followed by sulfurization. The kinetics and thermodynamics of the chemical process are pivotal factors influencing the growth of 2D materials.

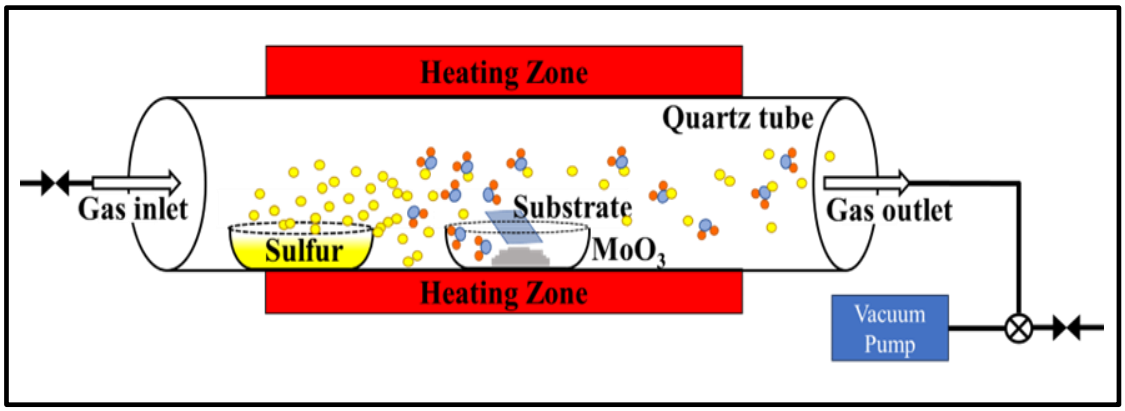

Figure 2.2 *Schematic illustration of CVD setup for the synthesis of MoS_2 film.*

In the present work, CVD technique has been used for the fabrication of varying morphologies (horizontally or vertically oriented) of MoS_2 over different substrates (SiO_2-Si, FTO, Si) using two solid precursors: (1) Molybdenum trioxide (MoO_3) and (2) sulfur powder (99%, Loba Chemie Pvt. Ltd., India). The setup for the CVD synthesis is shown in **Figure 2.2**. The single zone furnace consists of a quartz tube with the diameter of 5.5 cm and 1.0 m long, and two separate quartz crucibles are used for carrying the two precursors. A rotary pump is also attached to the CVD system for removing the impurities inside the tubular furnace and creating vacuum inside the tube. The (N_2) or (Ar + 10% H_2) gas are used as carrier gas. The flow rate of the carrier gas is controlled by using a ALICAT mass flow controller (MFC). Prior to growth, the substrates were separately cleaned in acetone and isopropanol for 10 minutes each using ultrasonic bath, and finally rinsed with deionized water. The MoO_3 powder was kept at the centre of the tubular furnace with clean substrate placed face down above the quartz boat containing MoO_3 powder and sulfur powder was placed upstream in the CVD system. Initially, vacuum was created multiple times to remove the trace gases present in the tube and the furnace was heated at a rate of 10 °C min^{-1}. Beside these parameters the Mo/S ratio and substrate choice

also plays a key role for governing the growth mechanism. At the reaction temperature, the sulfur vapors are carried by the carrier gas in the reaction zone, where it reacts with MoO_3 vapors to form volatile suboxide MoO_{3-x}. It further reacts with sulfur to form MoS_2. The growth process in thermal CVD is given by following chemical reactions [77, 78]-

$$MoO_3 + \frac{x}{2}S \rightarrow MoO_{3-x} + \frac{x}{2}SO_2 \quad (2.1)$$

$$MoO_{3-x} + \frac{7-x}{2}S \rightarrow MoS_2 + \frac{3-x}{2}SO_2 \quad (2.2)$$

Then it was allowed to cool down naturally to the room temperature. Distinct morphologies of MoS_2 may be ensued by different growth temperature, gas flow rate and reaction time, as shown in **Figure 2.3**. The different layered triangular (1L, 3L and 5L) MoS_2 over SiO_2-Si (SiO_2 thickness ~300 nm) substrate has been formed at ~700 °C in nitrogen atmosphere with flow rate of 100 sccm (Standard Cubic Centimeter per Minute) and reaction time of 5 min. In this growth process, two types of MoS_2 flakes have been recognized: one with the uniform planar thickness, that is, the monolayer, and the other with the central layered structure, i.e., three, five and above structures. These two types of MoS_2 formations are due to two different nucleation mechanisms, as described by Zhou *et al.* [79]. First is the two dimensional (2D) planar nucleation resulting from the lower reactant concentration on the substrate, leading to the growth of the monolayer. Second is the self-seeding nucleation that results from the higher reactant concentration, facilitating the growth of other layers. The growth of H-MoS_2/SiO_2-Si occurs at ~740 °C (ramping rate = 10 °C/min) in Ar/H_2 environment (flow rate = 100 sccm) with the reaction time of 10 min. The size of the randomly oriented MoS_2 triangular domains that are the nucleation sites for the horizontal growth, increases with growth temperature and longer reaction time and finally coalesce to form a continuous film. The V-MoS_2/SiO_2-Si has been obtained by raising the furnace at temperature ~750 °C (ramping rate = 10°C/min) in an Ar/H_2 environment (flow rate = 100 sccm) with the growth duration of 10 min. On SiO_2-Si substrate, the transition from horizontal to vertical growth is dictated by the relative vapor

amount of MoO_3 and S during growth process. Typically, a high S:MoO_3 concentration ratio and high temperature promotes the vertical growth, whereas a low S:MoO_3 concentration ratio and low temperature leads to horizontal MoS_2 growth [80, 81]. The formation of H-MoS_2/FTO occurs when the temperature of the furnace was gradually ramped to a growth temperature of ~720 ºC at a rate of 10 ºC/min. in Ar/H_2 gas mixture environment with a flow rate of 100 sccm. Since FTO substrate has a low melting temperature, so we chose little low reaction temperature to prevent the substrate deformation and for the new growth condition at low temperature, the growth time was increased to 20 minutes. The V-MoS_2/Si has been formed when the furnace temperature was gradually raised to ~750 °C (ramping rate = 10 °C/min) in an Ar/H_2 environment (flow rate = 100 sccm) with growth time of 10 min. The growth of vertically oriented MoS_2 on Si is promoted by the supersaturated MoS_2 vapor and sub-oxide compounds vapor. This is attributed to the increased diffusion rate and the dense nucleation sites of MoS_2 on Si substrate [82]. The convergence of two MoS_2 islands induces significant compression, causing distortion that forms an arch structure. This structural change alleviates the pressure, facilitating the vertical growth of MoS_2 on the Si substrate. **Figure 2.3** also shows the photograph of CVD synthesized triangular MoS_2, H-MoS_2/SiO_2-Si, V-MoS_2/SiO_2-Si, H-MoS_2/FTO and V-MoS_2/Si, indicating 0.9 × 0.5, 1.0 × 0.5, 0.9 × 0.5, 1.0 × 1.2 and 1.0 × 0.5 cm^2 growth region, respectively. The optical contrast shows the growth region and is mainly restricted by the diameter of the crucible. These distinct prepared MoS_2 nanostructures were analyzed using various characterization techniques ranging from microscopic to spectroscopic to examine their structural, vibrational and optical properties. The subsequent section outlines the array of characterization tools employed in this study.

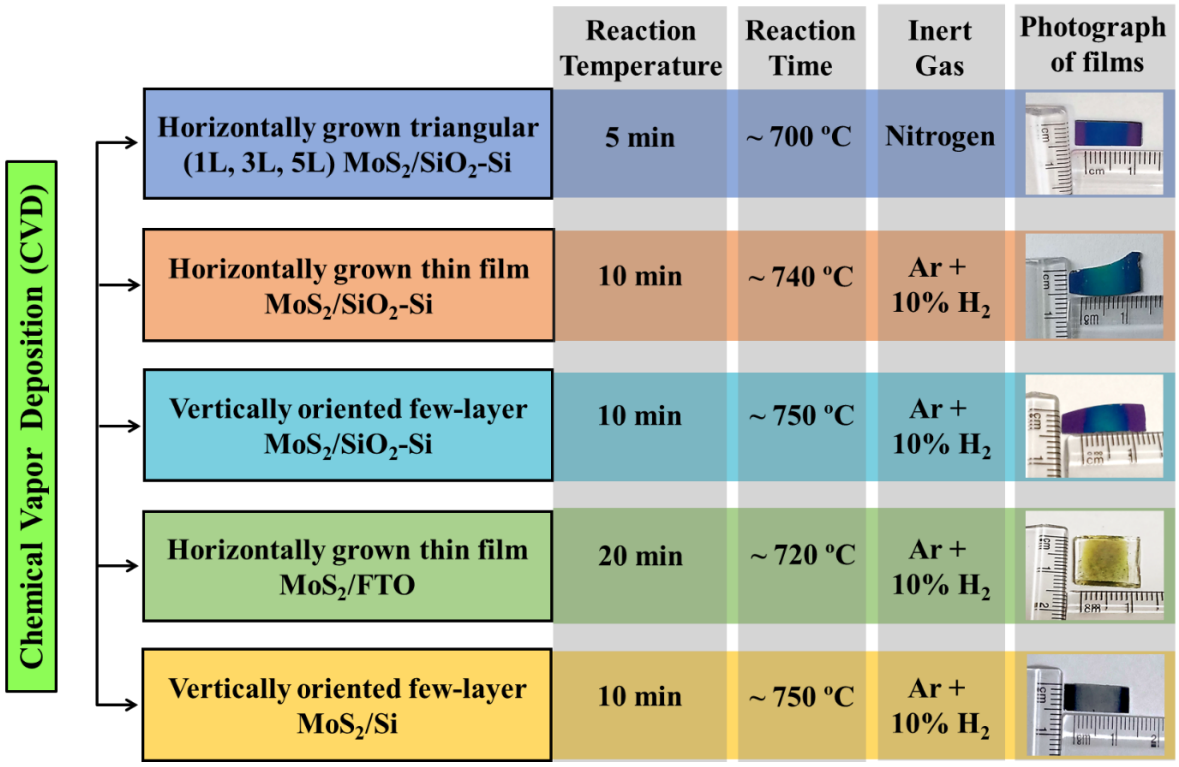

Figure 2.3 *Schematic outlining the different optimized MoS_2 films along with their growth conditions.*

2.2 Characterization Techniques

2.2.1 Optical Microscopy

Optical microscopy is a cornerstone technique in scientific research, enabling the visualization and analysis of specimens at the microscale. A contemporary optical microscope typically consists of essential components such as a light source, sample stage, condenser, objective lens, tube lens (eyepiece or ocular lens), detector and various light conditioning elements. A light source, often an LED or halogen lamp, emits light that is focused and directed onto the specimen through a series of lenses and mirrors. Usually, the sample is placed on a glass slide and is positioned onto the XYZ translational stage for microscopy. This stage enables precise focusing and positioning of the specimen during observation. **Figure 2.4** shows the schematic of the optical microscope.

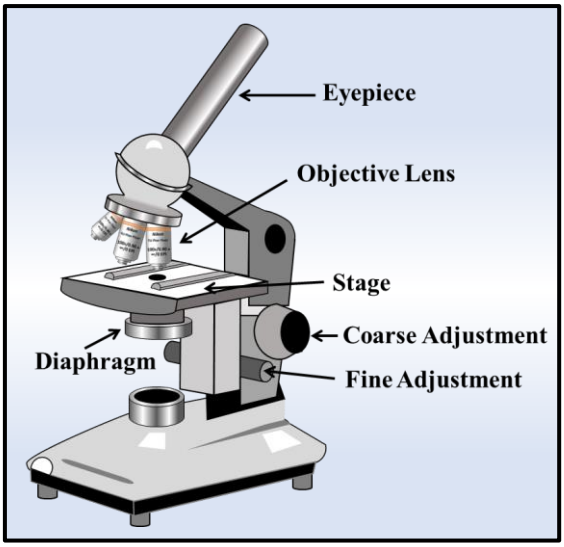

Figure 2.4 *Schematic diagram of optical microscope [83].*

Light passes through the objective lens, which is the primary lens closest to the specimen. This lens magnifies and collects light from the specimen. The objective lens plays an important role in determining key imaging factors such as numerical aperture, resolution and magnification. The numerical aperture (N.A.) of the objective lens quantifies its capacity to gather light and resolve fine features in the specimen. It is mathematically defined as -

$$N.A. = n \sin \theta$$

where n represents the refractive index of the medium and θ denotes the half-angle of the light collection cone. The microscope resolution (r) is the smallest resolvable distance between two distinct objects and is determined by Rayleigh's criterion -

$$r = 0.61 \lambda / N.A.$$

where λ represents the wavelength of light. Enhanced resolution relies on the capacity to register a greater number of higher diffracted orders into the objective lens. This means the higher numerical aperture in the objective lens corresponds to superior resolving capabilities of the system. As light passes through the objective lens, it creates an enlarged image of the specimen, that again passes through additional lenses, such as the tube lens or ocular lens (eyepiece). These lenses further magnify the image before it reaches the observer's eye or a camera. The observer views the magnified specimen through the eyepiece or via a camera

connected to the microscope. Adjustments to focus, illumination and magnification can be made to obtain a clearer and detailed image. The Nikon eclipse LV150N optical microscope is used in this study. **Figure 2.5 (a)** shows the optical image of different layered (1L, 3L and 5L) triangular MoS_2/SiO_2-Si, indicating 5-15 µm lateral dimension of each triangle of MoS_2. **Figure 2.5 (b, c)** shows the large-scale continuous growth of thin film of MoS_2 over SiO_2-Si and FTO coated glass substrates, respectively.

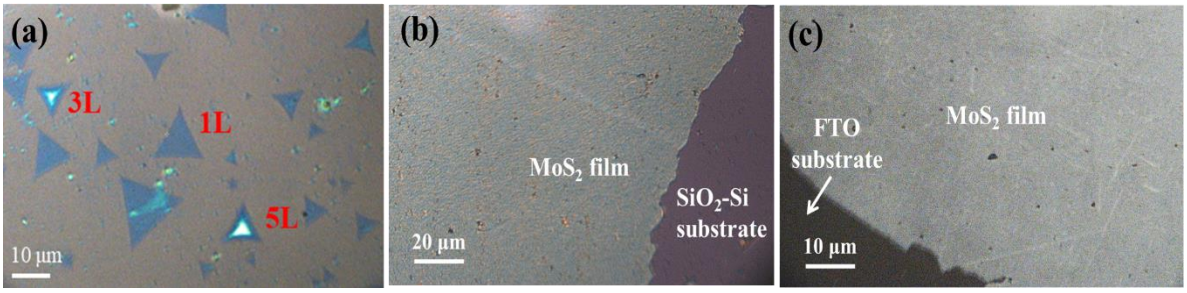

Figure 2.5 *Optical image of CVD synthesized (a) different layered (1L, 3L and 5L) triangular MoS_2/SiO_2-Si, (b) H-MoS_2/SiO_2-Si and (c) H-MoS_2/FTO.*

2.2.2 Scanning Electron Microscopy (SEM)

SEM is a highly versatile technique widely embraced by the scientific and engineering communities for observing the nanomaterial's surface morphology and structure. The Zeiss Supra-40 SEM was utilized to examine the morphology of prepared materials. In SEM technique, the high-energy electrons are focussed using different electromagnetic lenses to scan the specimen's surface. This focussed electron beam generates various signals at the surface of solid specimens, producing significantly higher resolution images compared to optical microscopy. **Figure 2.6** illustrates the typical layout of SEM, comprising of an electron gun for electron generation, an accelerating anode, electromagnetic lenses, vacuum system, motorized stage, secondary electron detector to capture emitted signals from materials and image display unit. When the electron beam interacts with the sample, a variety of signals are generated, including secondary electrons (SE), backscattered electrons (BSE), characteristic X-rays, etc. (**Figure 2.7**), offering insights into the sample's topography, composition and properties [84-

86]. In sample imaging, secondary electrons and backscattered electrons play vital roles. Secondary electrons are particularly useful for revealing morphology and topography details, showing surface features effectively. Conversely, backscattered electrons are useful in highlighting compositional contrasts within multiphase samples, facilitating rapid phase discrimination. The quality of SEM images relies on factors such as depth of field and resolution, influenced by parameters like working distance, probe current, accelerating voltage and astigmatism. Notably, SEM achieves resolutions within the nanometer range.

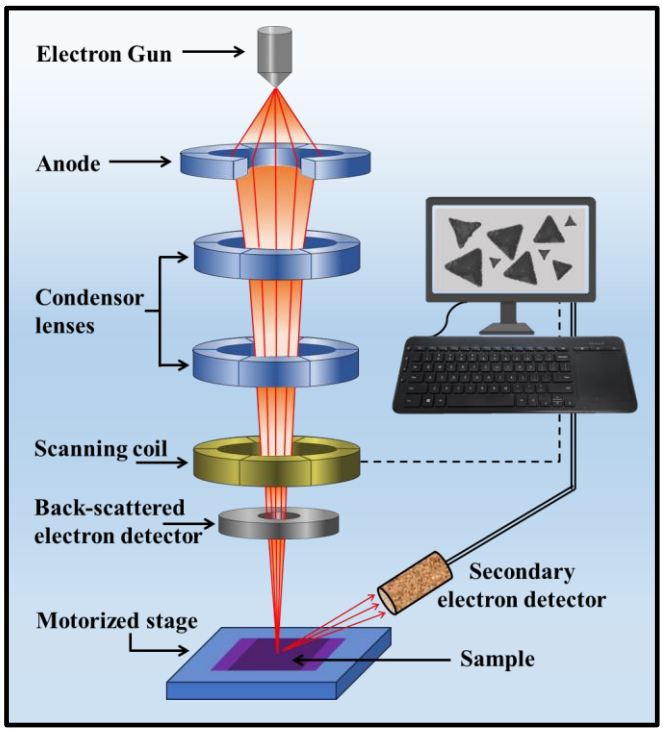

Figure 2.6 *Schematic diagram of scanning electron microscope (SEM) [87].*

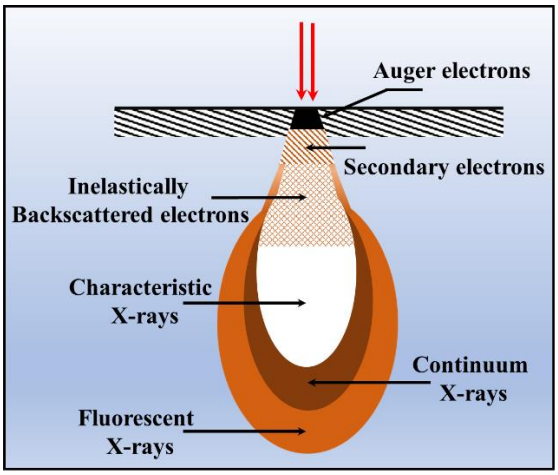

Figure 2.7 *Schematic showing the interaction of electron beam with sample in SEM [87].*

Figure 2.8 (a-e) shows the SEM images of different layered triangular MoS_2 grown over SiO_2-Si, H-MoS_2/SiO_2-Si, V-MoS_2/SiO_2-Si, H-MoS_2/FTO and V-MoS_2/Si, respectively. All the as-synthesized MoS_2 nanostructures on different substrates under different growth conditions illustrates the extensive surface area coverage and unique morphologies of the resulting films.

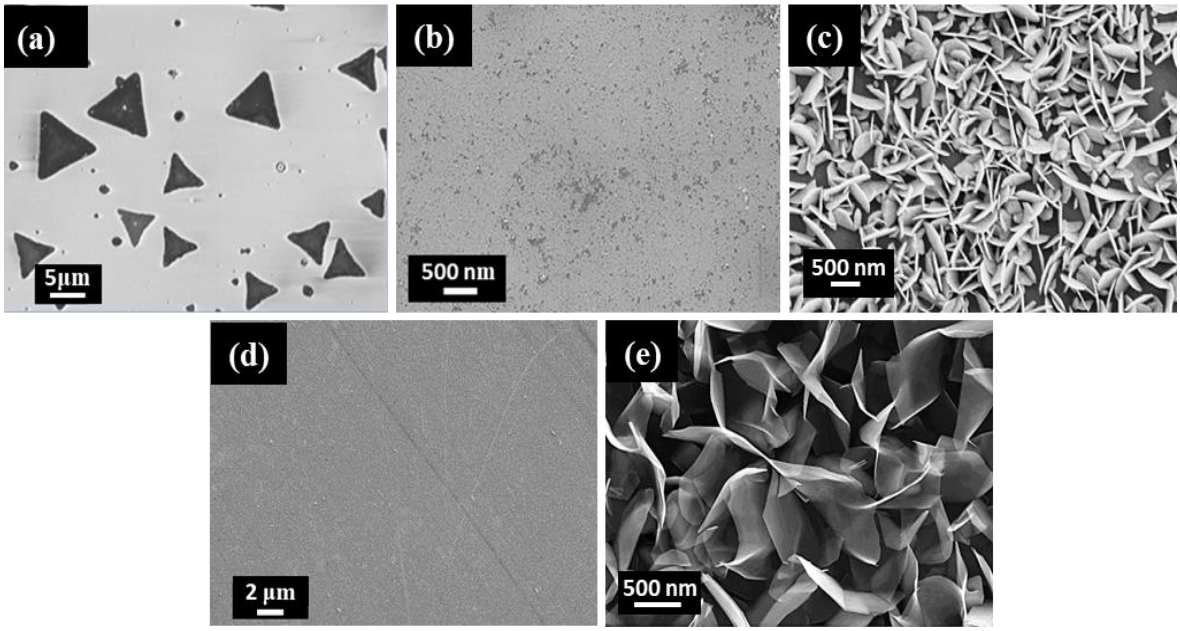

Figure 2.8 *SEM images of (a) different layered triangular MoS_2/SiO_2-Si, (b) H-MoS_2/SiO_2-Si, (c) V-MoS_2/SiO_2-Si, (d) H-MoS_2/FTO and (e) V-MoS_2/Si.*

2.2.3 Atomic Force Microscopy (AFM)

AFM are extremely versatile tool that characterizes the topography of nanomaterials by scanning the sample with a sharp nanometer probe. **Figure 2.9** shows the schematic of the AFM, consisting of a flexible cantilever, a sharp probe, laser, photodiode detector, piezoelectric scanner and a data processor [88]. The nanoscale probe is attached to the flexible cantilever, forming a spring arrangement. The cantilever dimensions typically fall within the micrometer range, while the tip's radius measures just a few nanometers. Varied cantilever lengths, shapes and materials result in different spring constants and resonant frequencies. Predominantly, probes are fashioned from materials like silicon nitride (Si_3N_4) or silicon (Si) [89]. The scanning of the sample by probe is monitored by piezoelectric scanner. As this tip moves across the sample, the interaction forces between the tip and the surface induce bending in the

cantilever. To measure this, a photodiode detector tracks the deflection of a laser beam reflected off the cantilever onto a segmented photodiode. Scanning in the AFM mode can be executed in three ways: contact, noncontact and tapping mode. In contact mode, probe scans the surface at a very low force and it experiences repulsive forces between the probe and the surface atoms, causing the cantilever to deflect. In non-contact mode, the tip of the cantilever hovers very close to, but doesn't touch the sample surface and is oscillated at a frequency slightly higher than its resonant frequency. The oscillation amplitude typically remains within a few nanometers, often less than 10 nm. In tapping mode, the cantilever oscillates close to its resonant frequency with an oscillation amplitude typically exceeding 10 nm, commonly ranging from 100 to 200 nm [91]. The signal is recorded by the computer to construct a detailed 3D image, illustrating the surface topography of the sample.

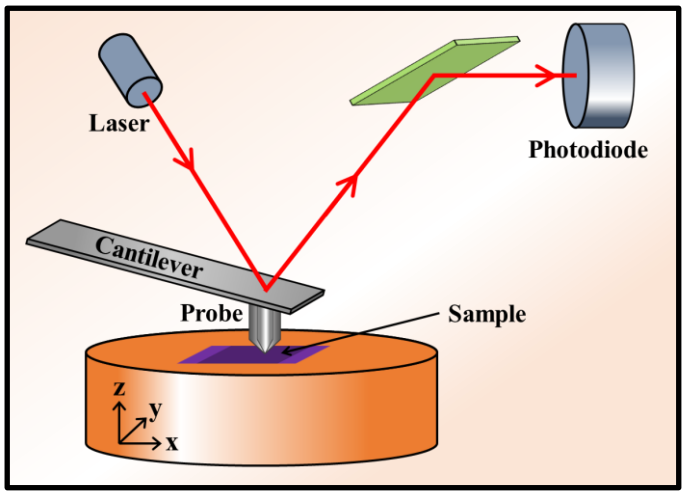

Figure 2.9 *Schematic diagram of atomic force microscope (AFM) [90].*

The AFM model NT-MDT (Russia) was used in this study. **Figure 2.10 (a)** shows the AFM image and corresponding height profile of 1L triangular MoS_2, with the thickness of ~0.8 nm, confirming the growth of 1L MoS_2. The AFM image of 3L triangular MoS_2 and its corresponding height profile showing thickness of ~2.4 nm, is shown in **Figure 2.10 (b)**. Similarly, the AFM image of 5L triangular MoS_2 and its corresponding height profile showing thickness of ~4.0 nm, is shown in **Figure 2.10 (c)**. **Figure 2.10 (d)** illustrates the AFM image

of H-MoS_2/SiO_2-Si, showing the clear boundary between MoS_2 and FTO substrate. The height profile along the blue line shows the film thickness of ~4 nm, suggesting five layers growth [92, 93]. **Figure 2.10 (e)** illustrates the AFM image and the corresponding height profile of H-MoS_2/FTO, showing film thickness of ~5 nm with surface roughness of 1 nm, suggesting presence of around seven layers growth [19].

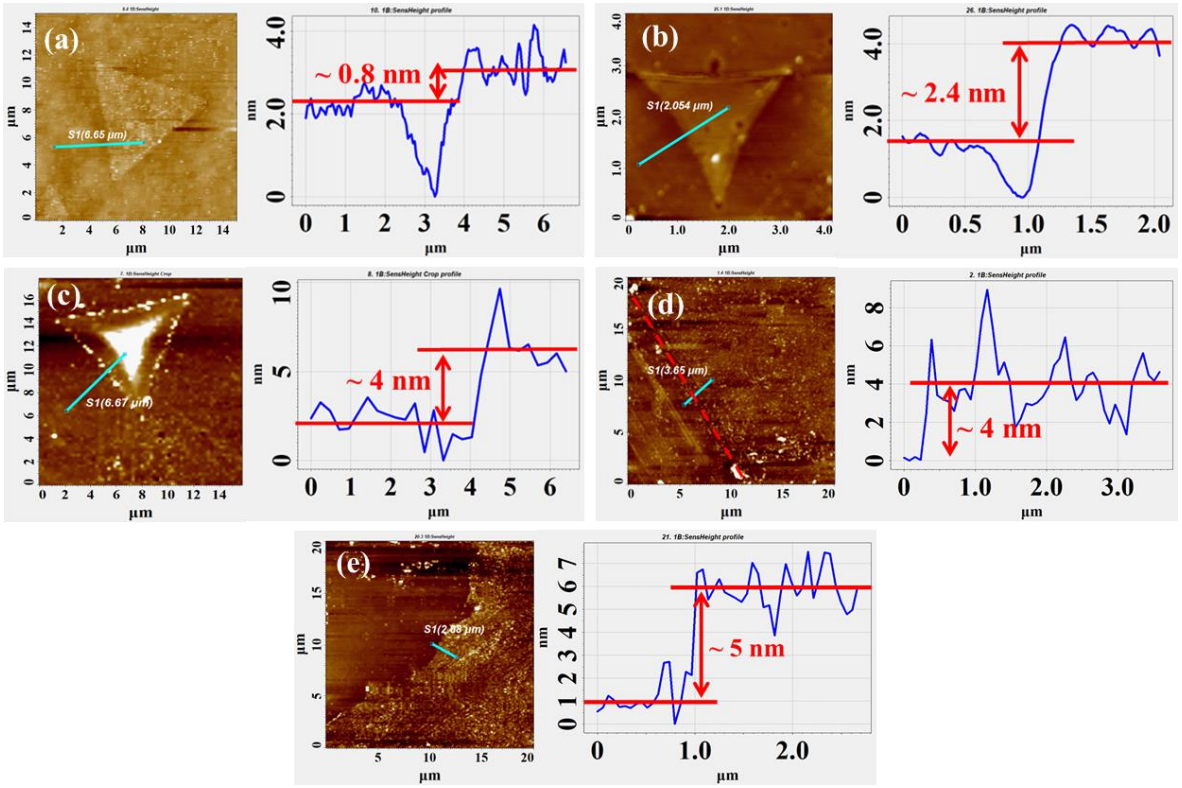

Figure 2.10 *The AFM image and corresponding height profile of (a) 1L, (b) 3L and (c) 5L triangular MoS_2/SiO_2-Si, (d) H-MoS_2/SiO_2-Si and (e) H-MoS_2/FTO.*

2.2.4 Raman Spectroscopy

Raman spectroscopy is a quick and non-destructive characterization tool, essential to study the chemical and physical properties of TMDs and other atomically thin 2D materials. It provides detailed information regarding chemical structure, phase, crystallinity and molecular interactions. In TMDs, Raman modes exhibit significant thickness-dependence, directly influenced in the frequencies of Raman modes. The incident electromagnetic field interacts with the sample, inducing a dipole moment that directly relates to the molecule's polarizability.

The induced dipole moment (μ_{ind}) is proportional to both the strength of the incident electric field (E_{in}) and the molecule's polarizability (α_m) and is given by [94]

$$\mu_{ind} = E_{in}(\omega_{inc}).\alpha_m \tag{2.3}$$

During interaction with the sample, incident light undergoes reflection, absorption and scattering. Raman spectroscopy utilizes the scattered light to get information about diverse vibrational modes. The predominant part of this scattered light constitutes elastic scattering, known as Rayleigh scattering. A minute fraction of this scattering light (~1 in 10^7 photons) constitutes inelastic scattering with optical frequency other than the incident photon frequency, as depicted in **Figure 2.11**.

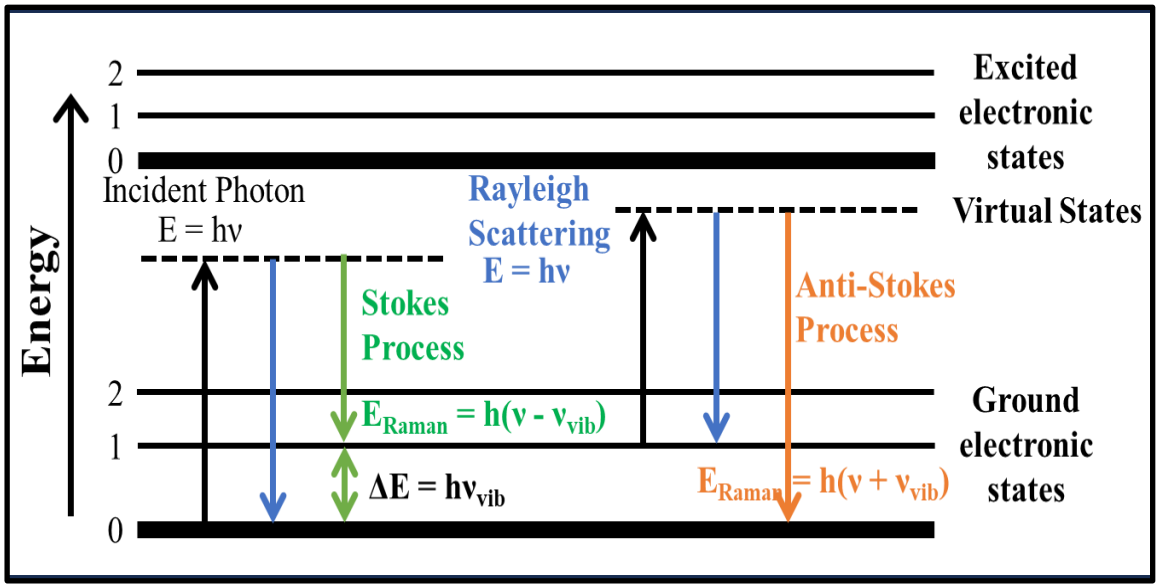

Figure 2.11 *Schematic representation of the various scattering process: Rayleigh, stokes and anti-stokes Raman scattering [95].*

Raman scattering comprises of both Stokes and Anti-Stokes scattering phenomena. The Raman spectrum illustrates the variation of scattered light's intensity with the Raman shift. The Raman shift is numerically given by-

$$\text{Raman Shift } (\nu) = \frac{1}{\lambda_{incident}} - \frac{1}{\lambda_{scattered}} \tag{2.4}$$

where $\lambda_{incident}$ and $\lambda_{scattered}$ are the wavelength of the incident and scattered light, respectively. We have used STR-300 micro-Raman spectrometer with 532 and 633 nm laser

excitation using 1200 and 2400 cm^{-1} gratings. The main components of Raman spectrometer are laser, sample chamber, spectrometer, and CCD detector, as shown in **Figure 2.12** [95]. To eliminate the Rayleigh signals, a notch filter is employed that allows the remaining signals to pass through a dispersive holographic grating. Adjustments in the intensity of the incident monochromatic laser source are managed using various neutral density filters. High-quality CCD detectors are utilized to capture and detect the Raman signal.

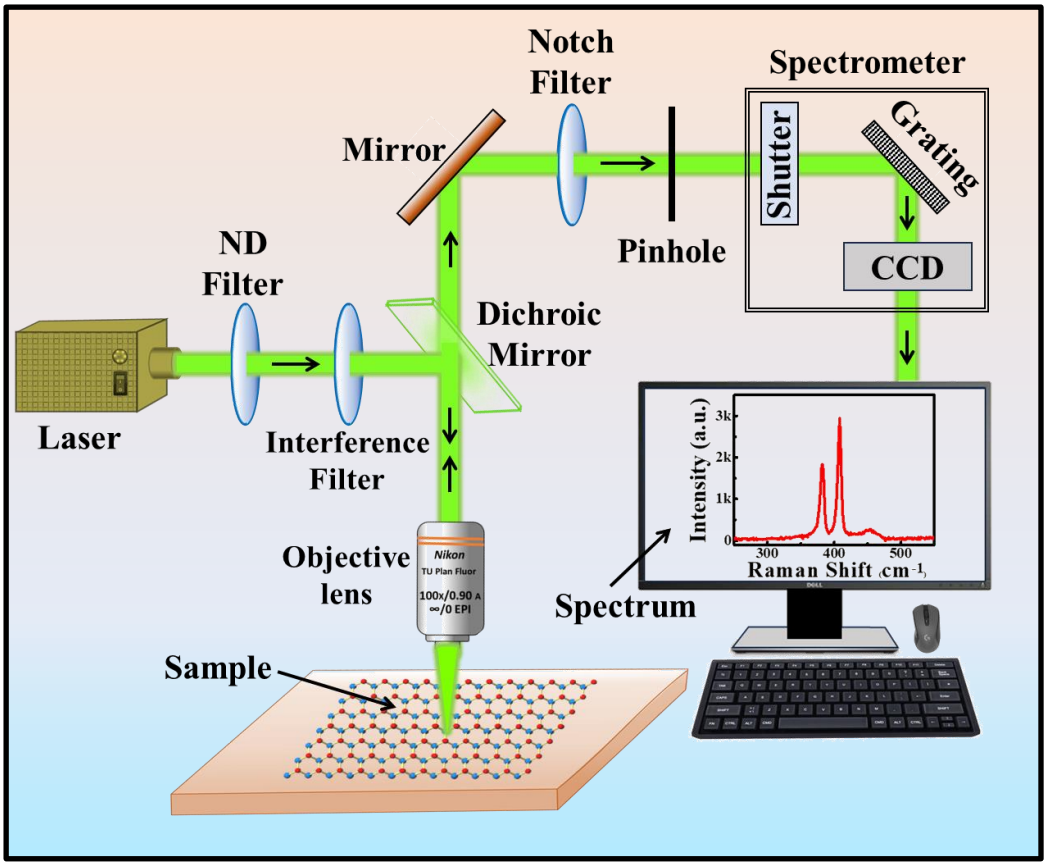

Figure 2.12 *Schematic diagram of Raman spectrometer.*

Figure 2.13 (a) displays the Raman spectra with 532 nm excitation of 1L, 3L and 5L triangular MoS_2/SiO_2-Si. The presence of two pronounced characteristic phonon modes: in-plane vibration of Mo and S atom (E^1_{2g}) and the out-of-plane vibration of S atom (A_{1g}) indicates the pure 2H phase of synthesized MoS_2 over different substrates. The separation between these two peaks features the estimation of layer number. Furthermore, a weak broad peak appears at ~450 cm^{-1} corresponding to 2LA(M) mode, a second-order longitudinal acoustic (LA) phonons

mode at M point in the Brillouin zone. **Figure 2.13 (b)** shows the Raman spectra of H-MoS_2/FTO, V-MoS_2/Si, V-MoS_2/SiO_2-Si and H-MoS_2/SiO_2-Si. **Figure 2.13 (c)** shows the resonant Raman spectra for 1L, 3L and 5L triangular MoS_2 with 633 nm excitation source. The intensity of different Raman modes enhances with increasing layer number in resonance Raman scattering due to strong electron-phonon coupling along z-axis. The Raman band at ~176 cm^{-1} and ~640 cm^{-1} are assigned as $A_{1g}(M)$ – LA (M) and $A_{1g}(M)$ + LA (M), respectively. Two peaks at ~383 and ~408 cm^{-1} are ascribed to $E^1{}_{2g}(\Gamma)$ and $A_{1g}(\Gamma)$ phonon modes, the same first-order bands as observed in non-resonant Raman spectrum. The peak at 227 and 454 cm^{-1} are assigned as LA(M) and 2LA(M) mode, respectively [96, 97]. **Figure 2.13 (d)** shows the Raman spectra for H-MoS_2/FTO, V-MoS_2/Si, V-MoS_2/SiO_2-Si and H-MoS_2/SiO_2-Si using 633 nm excitation.

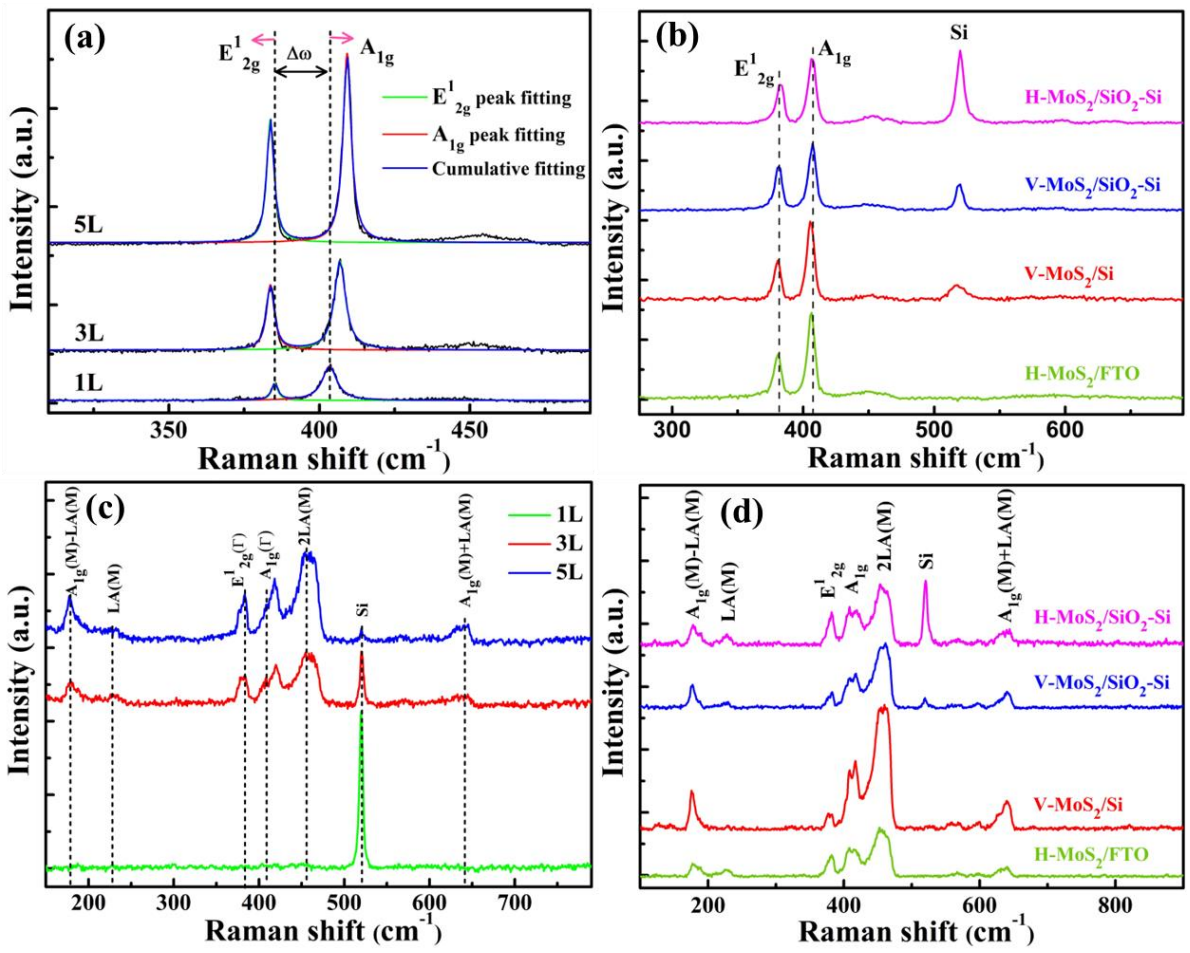

Figure 2.13 *Raman spectra of (a, c) 1L, 3L and 5L triangular MoS_2/SiO_2-Si and (b, d) H-MoS_2/FTO, V-MoS_2/Si, V-MoS_2/SiO_2-Si and H-MoS_2/SiO_2-Si, using 532 and 633 nm excitation wavelength.*

2.2.5 Photoluminescence (PL) Spectroscopy

The PL spectroscopy's versatility and non-invasive nature make it indispensable in exploring and optimizing various materials for applications in optoelectronics, photovoltaics, biomedical imaging and quantum information technologies. It provides valuable insights into bandgap energies, defect states, carrier dynamics and quantum efficiency, by analysing the emitted light's wavelength, intensity and decay times. This non-destructive method involves irradiating a sample with a light source, typically a laser, to initiate photoexcitation. Upon absorption of photons, electrons transition from their ground state to higher energy levels, creating electron-hole pairs or excitons. Subsequently, these excited electrons transit to the lowest energy of the excited state through a sequence of non-radiative transitions. As these excited states relax back to lower energy levels, the excess energy is emitted as photons, known as luminescence. The schematic showing the PL phenomenon is depicted in **Figure 2.14**. The emitted photons are collected and analyzed by a spectrometer. This instrument disperses the photons according to their wavelengths, allowing for the identification and quantification of emitted light, that carry information about the material's structure, composition and electronic characteristics. This technique offers high sensitivity and precision, enabling the characterization of nanoscale structures and individual quantum systems.

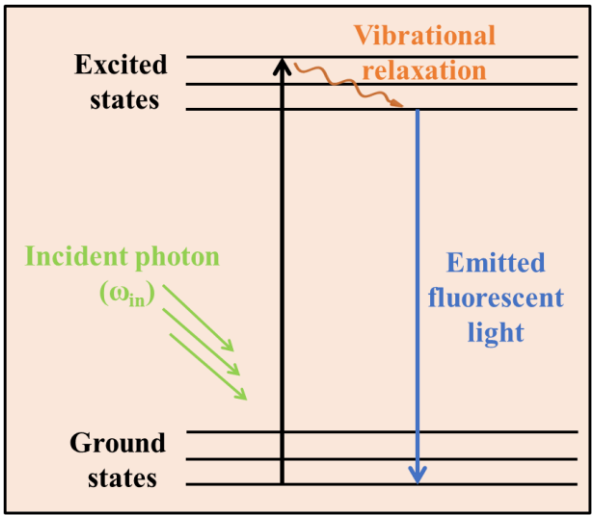

Figure 2.14 *Schematic representation of the photoluminescence (PL) spectroscopy [98].*

Figure 2.15 (a) shows the PL spectra of 1L, 3L and 5L triangular MoS_2/SiO_2-Si. Two main PL peaks appear at ~1.85 eV (A-exciton) and ~1.98 eV (B-exciton) are observed. This is ascribed to direct excitonic transition from split valence band (VB) owing to spin orbit coupling (SOC) to the doubly degenerate conduction band (CB) at K-point of the Brillouin zone and hardly changes with increasing layer number. The PL intensity for 1L is very strong and decreases with increasing layer number. **Figure 2.15 (b)** shows the PL spectra of H-MoS_2/FTO, V-MoS_2/Si, V-MoS_2/SiO_2-Si and H-MoS_2/SiO_2-Si. The PL peak positions of MoS_2 films grown over different substrates are affected by varying degree of strain of the underlying substrates and hence peak shifts are observed for MoS_2 grown over different substrates. For the case of different morphologies of MoS_2 grown over same substrate, i.e., for H-MoS_2/SiO_2-Si and V-MoS_2/SiO_2-Si, the horizontally grown MoS_2 film are in contact throughout the region with the substrate and hence are under maximal strain due to substrate, while the strain is minimal for vertically oriented (V-type) MoS_2 due to smaller contact area between MoS_2 and substrate [99]. Thus, the PL peak position of V-MoS_2/SiO_2-Si is observed to be slightly red-shifted compared to H-MoS_2/SiO_2-Si. The energy difference of ~0.13 eV is observed between these two excitonic peaks.

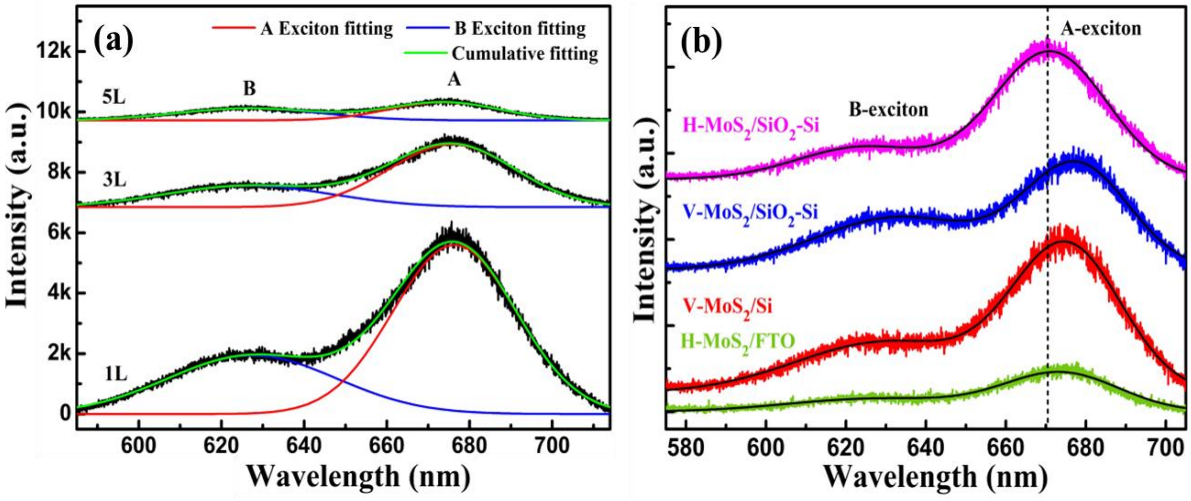

Figure 2.15 *PL spectra of (a) 1L, 3L and 5L triangular MoS_2/SiO_2-Si and (b) H-MoS_2/FTO, V-MoS_2/Si, V-MoS_2/SiO_2-Si and H-MoS_2/SiO_2-Si, using 532 nm excitation wavelength.*

2.2.6 UV-Visible Spectrophotometer

A UV-Visible spectrophotometer is an analytical instrument used to measure the absorption or transmission of light across the UV and visible spectrum by a substance. It's a crucial tool in chemistry, biology and materials science. The device emits a beam of UV or visible light through a sample and detects how much light is absorbed or transmitted. It consists of a light source emitting a broad spectrum of light, a monochromator selecting specific wavelengths, a sample compartment and a detector measuring light intensity, as depicted in **Figure 2.16**. The process begins with the light source emitting a beam passed through the monochromator to select desired wavelengths. This light passes through the sample and based on the substance's composition and concentration, certain wavelengths are absorbed. The detector then measures the intensity of light transmitted through the sample. By comparing the transmitted light intensity to the incident light intensity, the spectrophotometer determines the sample's absorbance or transmittance. These measurements aid in determining concentrations, identifying substances and studying molecular structure and properties in various scientific fields.

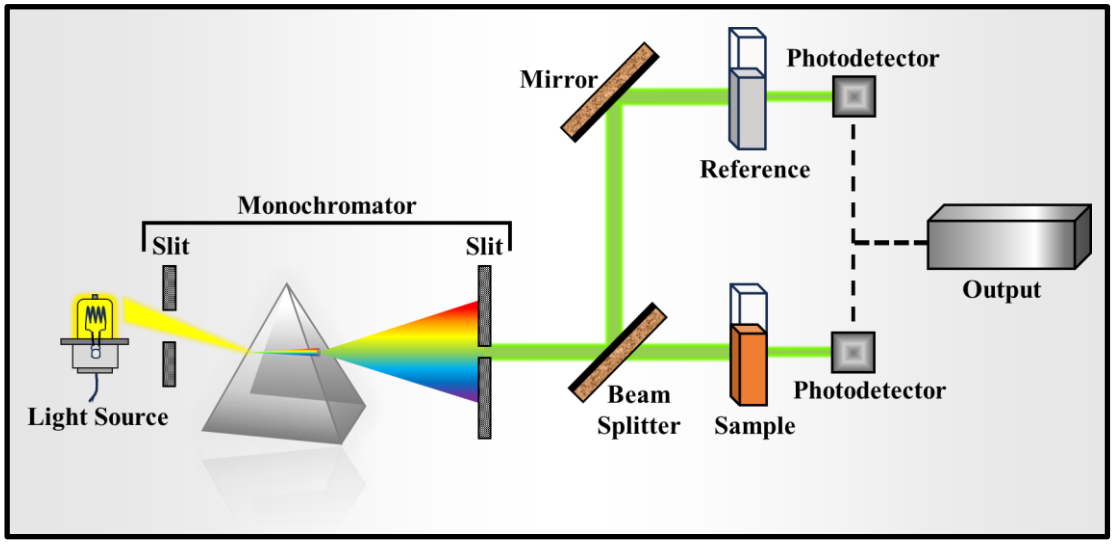

Figure 2.16 *Schematic diagram of UV-Visible spectrophotometer [100].*

Figure 2.17 shows the UV-vis absorption spectra of H-MoS_2/FTO, V-MoS_2/Si, V-MoS_2/SiO_2-Si and H-MoS_2/SiO_2-Si. Two prominent absorption peaks, namely A exciton and B exciton, are

consistently detected at ~677 nm and 626 nm, respectively, in MoS_2 samples grown on diverse substrates. These peaks signify direct excitonic transitions resulting from the spin-orbital splitting of the VB to the CB's minimum. Additionally, the spectra exhibit a broader peak spanning the range of approximately 400-600 nm, indicative of electron transitions occurring between regions characterized by higher densities of states.

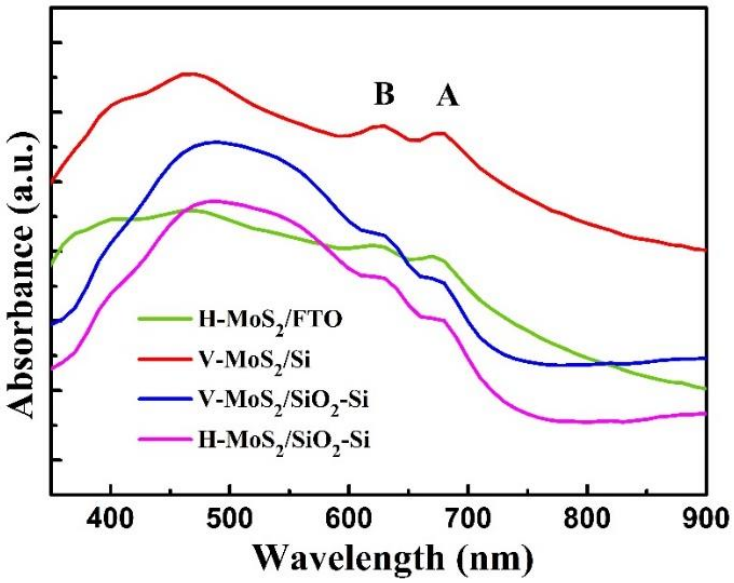

Figure 2.17 *UV-vis absorption spectra of H-MoS_2/FTO, V-MoS_2/Si, V-MoS_2/SiO_2-Si and H-MoS_2/SiO_2-Si.*